AIAA JOURNAL
Vol. 35, No. 3, March 1997

Measurements of the Velocity and Turbulence Structure of a Rotor Tip Vortex

Yong Oun Han*
Yeungnam University, Gyongsan 712-749, Republic of Korea
and
J. Gordon Leishman† and Alan J. Coyne‡
University of Maryland, College Park, Maryland 20742

The turbulent flow structure of a tip vortex generated by a hovering rotor was investigated with the use of three-dimensional laser Doppler velocimetry. The velocity field was measured at five wake ages, with the three components of turbulence being measured at the three earliest ages. The tangential (swirl) velocity component inside the tip vortex was found to have a self-similar behavior for all wake ages. The viscous core size was estimated to be approximately 2.5% of the blade chord just after formation, growing with the square root of vortex age to about 13% of blade chord at one rotor revolution. At early wake ages, radially symmetric peaks in the turbulence intensities were measured inside the vortex core, whereas only a single peak appeared in the turbulence distribution at later ages. The radial component of turbulence was found to be the most dominant, with the axial component being the smallest. Additional turbulence quantities, such as Reynolds' stress, were also measured. Finally, the evolutionary features of the turbulent kinetic energy production are discussed.

Nomenclature

c	= rotor blade chord, m
$\underline{P}$	= production rate of turbulent kinetic energy, m^2s^{-3}
$\overline{q^2}$	= turbulent kinetic energy, m^2s^{-2}
R	= rotor radius, m
r, θ, z	= vortex coordinate system
$\bar{r}$	= nondimensional vortex radius, r/r_c
r_c	= vortex core radius, m
r_0	= initial vortex core radius, m
S_{ij}	= mean strain rate, s^{-1}
s_{ij}	= fluctuation of mean strain rate, s^{-1}
t	= time, s
U_i	= mean velocities; V_r, V_θ, V_z for $i = 1, 2, 3$, ms^{-1}
u, v, w	= swirl, radial, and axial turbulence components, respectively, ms^{-1}
$\overline{u_i u_j}$	= Reynolds' stress, m^2s^{-2}
V_r	= radial velocity, ms^{-1}
V_{tip}	= rotor tip velocity, ΩR, ms^{-1}
V_z	= axial velocity, ms^{-1}
V_θ	= tangenetial (swirl) velocity, ms^{-1}
x_r, y_r, z_r	= rotor hub coordinate system, m
Γ	= circulation, m^2s^{-1}
$\bar{\Gamma}$	= average circulation around the vortex, m^2s^{-1}
$\underline{\delta}$	= nondimensional scaling factor ($\ll 1$)
δ	= apparent viscosity coefficient
ϵ	= dissipation rate of turbulent kinetic energy, m^2s^{-3}
ζ	= wake age, deg
ν	= kinematic viscosity, m^2s^{-1}
ρ	= air density, $kg\,m^{-3}$
ψ	= blade azimuth angle, deg
Ω	= rotor rotational frequency, rad s^{-1}

Introduction

THE blade tip vortices are the most distinct three-dimensional flow features generated by rotary wings. Unlike a fixed-wing aircraft where the wing tip vortices are quickly swept downstream, rotor tip vortices remain close to the plane of the rotor for a considerable time. Their high strengths and proximity are such that they can significantly affect the aerodynamic loads produced on following blades. This has a fundamental impact on metrics such as overall vehicle performance, rotor vibratory loads, blade aeroelasticity, and rotor noise generation. Understanding the physics of vortex formation, the viscous core size, radial distribution of swirl velocity, as well as diffusion and dissipative mechanisms, will have a fundamental impact on the ability to predict these metrics and minimize adverse vortex induced effects. An improved understanding of rotor tip vortices is imperative to help understand the aeroacoustic problems associated with blade vortex interaction (BVI)[1,2] and the large unsteady airloads produced by rotor wake/airframe interactions.[3,4]

When a vortex is created at a rotor blade tip it only remains laminar for a short time. Thereafter, it rapidly becomes turbulent with an enlarging core radius as a result of viscous diffusion. In previous measurements with vortices,[5,6] an energetic turbulent behavior has been observed along the viscous core boundary, even in the early stages of formation. These turbulent actions transmit through the vortex and eventually serve to attenuate the vortex through dissipation. Much of what is known about turbulent vortices has been obtained from experiments with rectilinear tip vortices.[6–13] The tip vortex structure generated by rotors is less clear, but aspects of the rotor wake and tip vortex structure have been unveiled by various techniques including hot-wire anemometry,[5,10,14,15] flow visualization,[15–19] and laser Doppler velocimetry (LDV).[20–25]

One advantage of LDV is that it is nonintrusive, and so unlike a conventional probe it will not disturb the flow and alter the evolutionary physics of diffusion and dissipation. Several techniques have been developed for making turbulence measurements with LDV in quasisteady vortex flows.[26–28] Also, whereas the tip vortex turbulence structure has been examined in some detail for fixed wings using LDV,[29,30] there is a dearth of corresponding measurements for rotating wings. This is partly because of resolution difficulties and the need to acquire large numbers of statistically valid samples to allow satisfactory phase averaging of periodic rotor flows. Vortex measurements are also difficult, in general, because of the characteristic wandering features observed with rectilinear vortices.[11,12] Furthermore, seeding is critical for LDV measurements.[31] Because of the inertial and viscous drag forces that act on the seed particles, they are not easily coaxed into the vortex cores, especially when the vortices are young and have high-swirl velocities.[32]

Received July 19, 1996; revision received Oct. 17, 1996; accepted for publication Oct. 21, 1996; also published in *AIAA Journal on Disc*, Volume 2, Number 2.

*Professor, Department of Mechanical Engineering. Member AIAA.
†Associate Professor, Center for Rotorcraft Education and Research, Department of Aerospace Engineering. Senior Member AIAA.
‡Rotorcraft Fellow, Center for Rotorcraft Education and Research, Department of Aerospace Engineering. Member AIAA.

The present study reports the first phase of a detailed investigation of rotor tip vortices in their early stages after formation. Coincident three-dimensional LDV measurements were conducted in the wake of a single-bladed rotor system, allowing a unique opportunity to examine the generated tip vortex for up to one revolution prior to interference effects at the first blade passage. This article focuses on measurements of the velocity field and turbulence structure in the tip vortex and is directed toward uncovering a better physical understanding of the tip vortex formation and its subsequent behavior as it is convected away from the rotor.

Description of the Experiment

A tip vortex with a nominally helical trajectory was generated by a rotor with a single blade. This untwisted blade was rectangular in planform with a 40.6-cm radius and 4.25-cm chord and used a NACA 2415 airfoil section. The blade was mounted on a teetering type hub and balanced by a counter weight. The rotor assembly was mounted horizontally in a large test cell, thereby minimizing floor/wall interference or recirculation effects. A three-phase variable frequency motor was used to drive the rotor at 2100 rpm, giving a tip Mach number of 0.29 and a tip Reynolds number of 2.5×10^5. The collective pitch was maintained at 4 deg, giving a nominal nondimensional tip vortex strength[20] $\bar{\Gamma}/(c\Omega R)$ of 0.16 and a vortex Reynolds number Γ/ν of 4×10^4. The rotational speed and phasing was monitored by an angular resolution sensor keyed to the rotor shaft. This sensor also triggered a data link unit that encoded rotor azimuth information with the LDV measurements.

Three velocity components were measured using a fiber-optic-based LDV system. This system comprised a 6-W argon-ion laser source, beam separators, a matrix of fiber-optic couplers, transmitting optics with beam expanders, and coaxial receiving optics. The six beams (two colors for each velocity component, with one of each pair being frequency shifted) were focused at a point in the rotor wake. The LDV measurement volume was defined by three pairs of intersecting ellipsoids with approximate dimensions of 73 μm in diameter by 0.85 mm long (based on the Gaussian $1/e^2$ points at $\lambda = 488.0$ nm) and contained 24.3 fringes. The actual measurement volume, however, was approximately spherical with a diameter equal to the minor axis of the ellipsoids, roughly 70 μm in this case. Note that with the present setup the individual channels did not directly measure three orthogonal velocities, and so it was necessary to resolve the velocity components based on the beam crossing angles. The measurement volume was moved by traversing the entire optics package in three orthogonal directions by using a computer controlled traverse (see Fig. 1).

Seeding was obtained using atomized olive oil that was entrained naturally into the rotor flow from an atomizer located just upstream and outside of the rotor slipstream. The seed particles had a specific density of 0.91, with the average particle size being 0.8 μm.

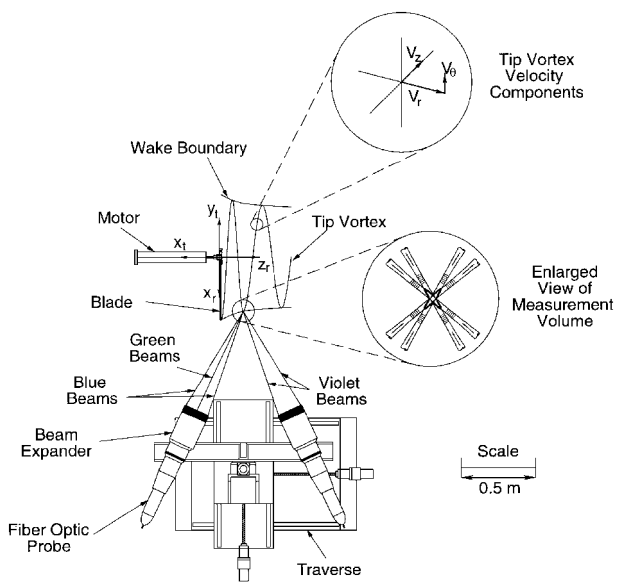

Fig. 1 LDV system and rotor, with rotor and vortex coordinate systems.

The signals produced by scattered light were received by the optics and led via fiber-optic cables to a set of photomultiplier tubes, converted into digital form, and then conditioned by a digital burst correlator (DBC). The data link unit was interfaced to the DBC; the unit ensured that all of the data was obtained in a phase-locked sense and also tagged azimuth information to the data. These data were then sorted into discrete azimuth bins. All measurements were made in coincidence mode, which meant that all three processors had to measure the velocity of the same particle within a defined coincidence window. Coincidence mode ensures correlated velocity components and is essential for turbulence measurements.

Because of the axisymmetric nature of a rotor wake in hover, the convecting tip vortex could be captured by making measurements over a set of one-dimensional radial grids parallel to the rotor tip-path plane and perpendicular to the main slipstream (z_r axis). At some rotor azimuth angle (wake age) the vortex axis becomes fully centered on one of these grids. Because of the helical pitch and radial contraction of the vortex, this resulted in measurements taken over grids that were not quite perpendicular to the vortex axis. However, the rotor is lightly loaded, and the helical pitch of the tip vortex is low. Estimates of the crossing angles were found to be less than 2 deg in all cases,[20] and so the nonorthogonality plays no significance in the measured data. Because of the high temporal resolution of these experiments, there were several bins of data close to the vortex core/grid crossing condition. The final data (bin) was selected by an analysis of the velocity gradients near the crossing point. A grid with a 2-mm spacing was used outside the vortex core region, but as the measurement point approached the vortex core the grid spacing was decreased to 0.2 mm. Each radial measurement grid at each wake age contained up to 86 points. The measurements were made at five wake ages, $\zeta = 17$, 51, 102, 232, and 311 deg.

Initial experiments were run to acquire a full revolution of 400 bins of data at each grid point. For these phase-resolved measurements, 20,000–40,000 coincident data samples per channel per grid point were specified. After the vortex core/grid crossing bin was verified, as already explained, a second test was conducted to window the measurements into only part of the azimuth. Typically, 20,000–40,000 data points were now windowed down to only 30 azimuth bins (approximately 27 deg of rotor azimuth), with approximately 15 bins on either side of the vortex/grid crossing bin. Windowing allowed a much larger number of samples to be obtained in each bin (on average about 10,000 samples), improving the statistical accuracy. However, the fundamental difficulties in entraining seed particles into the vortex core still reduced the number of valid samples when $\bar{r} < 0.25$. For further details on seeding issues and velocity bias in vortex flows, see Ref. 32.

Results and Discussion

Tangential (Swirl) Velocities

In Fig. 2 the measured tangential (swirl) velocities for the five wake ages are plotted with respect to the rotor coordinate system. The vortex was found to form almost precisely at the blade tip and

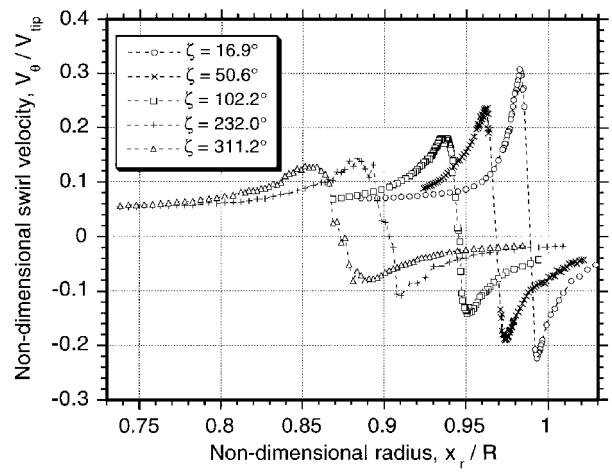

Fig. 2 Phase-averaged swirl velocity components of vortex at different wake ages; rotor coordinate system.

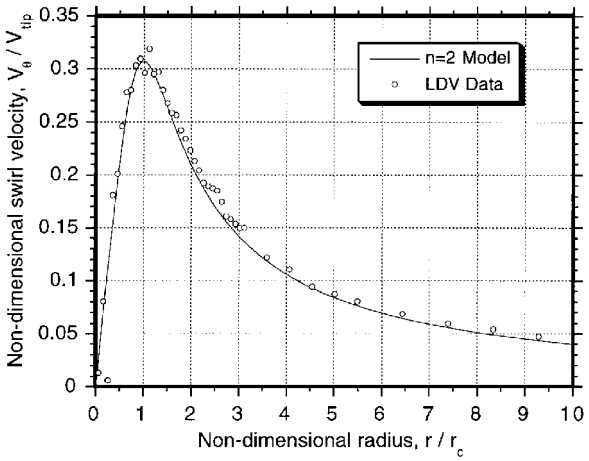

a) Plot inside rotor slipstream

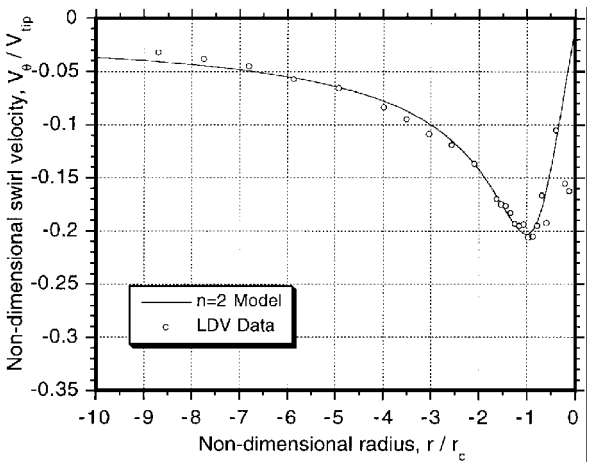

b) Plot outside rotor slipstream

Fig. 3 Swirl component of vortex perturbation velocity compared with $n = 2$ algebraic model at $\zeta = 16.9$ deg.

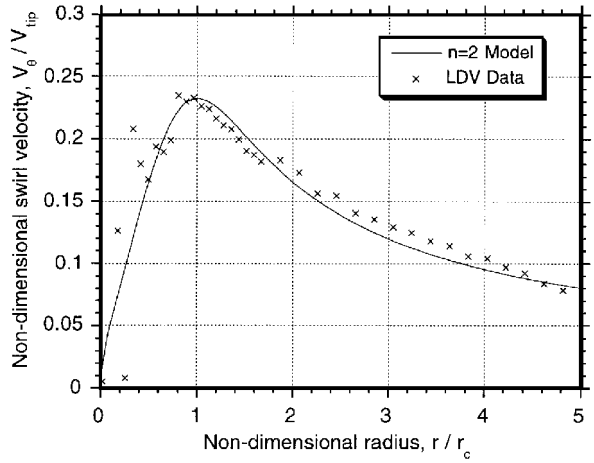

a) Plot inside rotor slipstream

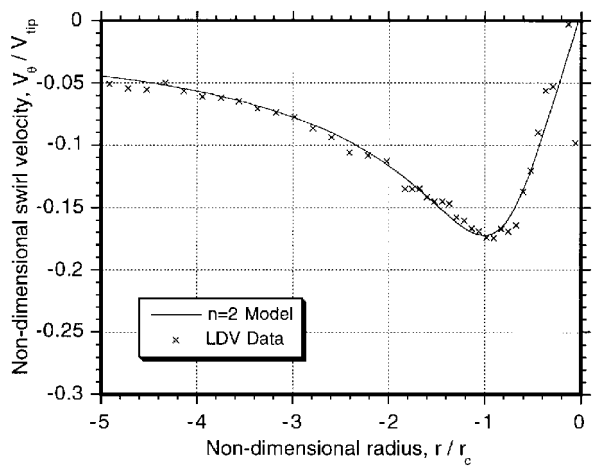

b) Plot outside rotor slipstream

Fig. 4 Swirl component of vortex perturbation velocity compared with $n = 2$ algebraic model at $\zeta = 50.6$ deg.

was then convected axially downward (in the z_r direction) away from the rotor plane and radially inward. During this process it is seen from Fig. 2 that the peak swirl velocities diminished and the viscous core region enlarged. This is a consequence of viscous diffusion. As expected, because the vortex is convecting axially through the flow, an asymmetric velocity behavior was measured with respect to the vortex core.[18,20,33,34] This is compounded because of the higher axial velocities found inside the rotor slipstream, thereby giving a significant time-averaged velocity gradient across the wake boundary. In addition, there is an asymmetry produced because of the vortex curvature (similar to that obtained with a vortex ring[18,35,36]) with a nonzero velocity also being produced at the vortex core.

To allow a further analysis of the vortex profile, the convection velocity was removed by subtracting the time-averaged flow velocities over one rotor revolution at the same grid points from the phase-averaged velocities, thereby leaving a residual or perturbation velocity field. These data are shown in Figs. 3–5. The remaining asymmetry of the vortex profile is because of the self-induced effects of curvature and contraction of what is an almost helical filament.[20]

A detailed analysis of the perturbation velocity profile was conducted in a previous experiment,[20] where the tangential (swirl) velocity component was found to be closely approximated by the $n = 2$ case of the series of two-dimensional algebraic profiles given by Vatistas et al.,[37] where

$$V(\bar{r}) = \frac{\bar{\Gamma}}{2\pi r_c}\left[\frac{\bar{r}}{(1+\bar{r}^{2n})^{1/n}}\right] \tag{1}$$

and where $\bar{r}$ is the nondimensional radius based on the estimated core radius r_c. Note that with $n = 1$ the Kaufmann or Scully vortex model is obtained, and as $n \longrightarrow \infty$ the Thompson–Rankine vortex is recovered. The results were also found to be quite well approximated by the Lamb–Oseen vortex model,[38] where

$$V_\theta(\bar{r}) = \frac{\bar{\Gamma}}{2\pi r_c \bar{r}}[1 - \exp(-\alpha \bar{r}^2)] \tag{2}$$

with $\alpha = 1.25643$.

To illustrate the quality of the fit to these two-dimensional models, results for the Vatistas et al.[37] $n = 2$ case are plotted against the measured data, as shown in Figs. 3–5. (Other comparisons are shown in Ref. 20.) The agreement with the $n = 2$ case is good, confirming that the profile maintains its self-similarity, at least in the early ages of development. This is important for rotor analyses, for example, using vortex free-wake models, such as Refs. 36, 39, and 40, where a vortex induced velocity model must be provided.

Vortex Core Growth

The average core radius of the tip vortex generated by helicopter rotors has been previously estimated to be of the order of the blade thickness,[15,18,19] which is typically 5–15% of mean blade chord. As the tip vortices generated by each individual blade evolve, they interact with each other and distort both in spatial position and in profile distribution under the action of their self- and mutually induced velocity fields. In addition, the closeness of following blades to vortices trailed from previous blades may cause perturbations to the vortex flow and may significantly alter its structure and evolutionary trends. Therefore, in the present experiment the use of a one-bladed rotor allowed a rare opportunity to study a helical vortex for a much longer wake age in the absence of such effects.

The Lamb–Oseen vortex velocity profile already given satisfies the Navier–Stokes equations. The variation of the core radius r_c with time can be shown to vary with the square root of vortex age.[41–43]

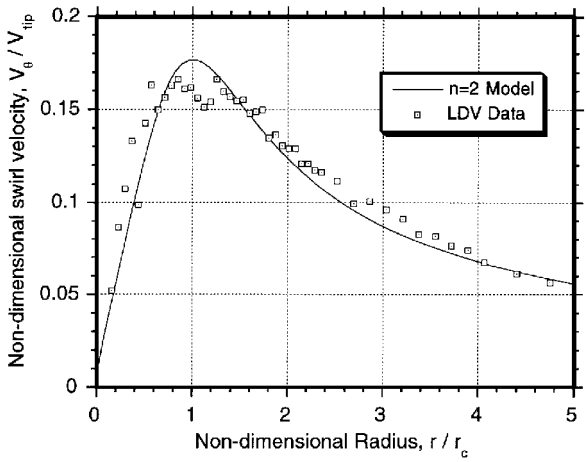

a) Plot inside rotor slipstream

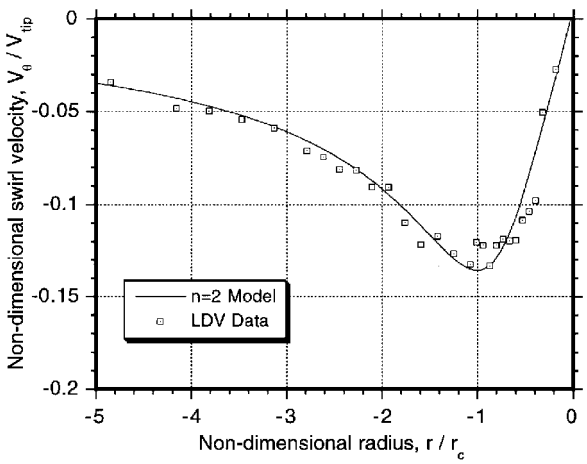

b) Plot outside rotor slipstream

Fig. 5 Swirl component of vortex perturbation velocity compared with $n = 2$ algebraic model at $\zeta = 102.2$ deg.

Because of turbulence generation, however, the actual diffusion of vortices is known to be much quicker than that based on laminar flow assumptions. To account for this, an average apparent or virtual viscosity coefficient δ can be used,[38,43–45] such that $\delta\nu = \text{const}$, where δ is empirically determined. This assumption is frequently made in wakes and jets.[46] For rotor applications, the vortex age can be measured in terms of rotor azimuth, so that using the value of ν for air and simplifying gives for the core growth

$$r_c = r_0 + 0.00855\sqrt{\delta(\zeta/\Omega)} \tag{3}$$

where r_0 is some initial core size and ζ is measured in radians.

Like the induced velocity model, a model of the core growth must also be provided empirically for rotor free-wake analyses. Estimates of measured growth of r_c with wake age, based on the least-squares fits to the Vatistas et al.[37] $n = 2$ model and the Lamb–Oseen model, are shown in Fig. 6. Two extra points at $\zeta = 89$ and 191 deg are also shown. The initial core size was estimated by extrapolating back to zero age, in this case $r_0/c = 0.025$. Results from Eq. (3) are also shown for different values of δ, from which it is apparent that the laminar decay ($\delta = 1$) of the vortex is indeed unrealistically slow. Here, it appears that $\delta \approx 10$, and this is consistent with measurements for fixed-wing vortices but at a somewhat lower vortex Reynolds number; see, for example, Dosanjh et al.[44]

It should be appreciated that the value of δ will be considerably larger for full-scale rotors, which will have vortex Reynolds numbers that are at least one order of magnitude greater than those measured here. However, the quantitative effects of vortex Reynolds number on the virtual viscosity coefficient of rotor vortices is still unknown and must remain the subject of future study.

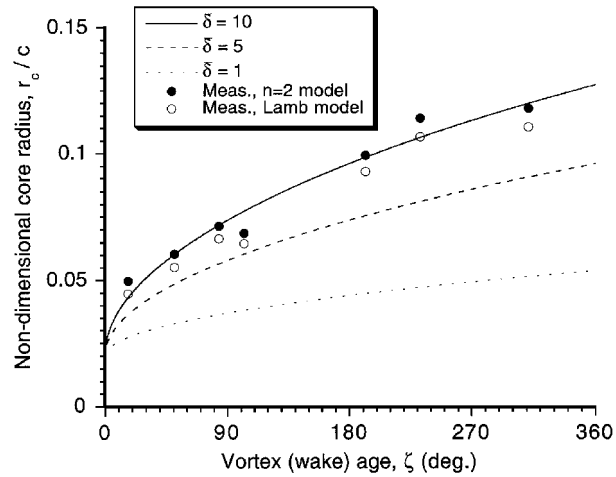

Fig. 6 Estimated vortex core growth vs wake age.

Circulation Profiles

Using the measured swirl velocity, the circulation around the tip vortex was calculated numerically around a circular curve that enclosed the vortex flow, i.e.,

$$\Gamma(r) = \int_0^{2\pi} V_\theta(r) r \, d\theta \tag{4}$$

The circulation values can be considered separately for the outer (outside rotor wake) and inner (inside rotor slipstream) parts of the induced velocity field on a plane perpendicular to the vortex axis, with the net circulation obtained from the average of these results. The net circulation around the vortex $\bar{\Gamma}$ was found to remain nominally constant during the first rotor revolution.[20]

In Fig. 7 the circulation profiles are plotted for the inner (rotor slipstream) side of the tip vortex. The steep gradients confirm that most of the vorticity is contained inside the core, although the asymptotic nature of the circulation distribution confirms that the flow is not irrotational immediately outside the core region. The circulation profiles showed fairly self-similar profiles on the basis of the $n = 2$ swirl velocity model, as discussed earlier. Compared to the Tung et al.[5] result for the circulation profile, however, the present results showed a much more rapid growth in circulation when moving away from the vortex axis. The milder slope in the circulation profiles of Tung et al.[5] could be caused by the limited spatial resolution of hot-wire sensors in regions where the velocity gradients are steep. The three normalized circulation profiles confirmed that there was a strong two-dimensional self-similarity in the swirl component of velocity field during the early stages of the tip vortex formation and its convection through the flow.

Axial Velocities

The axial velocities in the vortex core were found to be small in magnitude relative to the swirl velocities, yet the results were noted to take on a very characteristic profile, as shown in Fig. 8, for the first three wake ages. The sign of the axial velocities are such that a wakelike flow exists inside the core region. For a viscous laminar vortex, the axial velocity distributions are given by Lamb[38] as

$$V_z(r, t) = (A/t)\exp(-r^2/4\nu t) \tag{5}$$

where A is a constant that can be related to the drag on the rotor blade.[43] Other possible axial velocity distributions are discussed by Vatistas et al.[37] The Lamb result predicts that the axial velocity should diminish in proportion to ζ^{-1}, which is fairly consistent with observed behavior. Recall that the tangential component (which is much larger in magnitude) also diminishes with the inverse of wake age, but at a much lower rate. Unlike the swirl component of velocity, the axial velocity component measured here did not show a strong self-similar behavior.

Examination of axial velocity profiles also revealed that there were small but significant perturbations just outside the primary vortex core at all three wake ages. The reason for this is not completely clear, but it may be because of secondary vortical structures

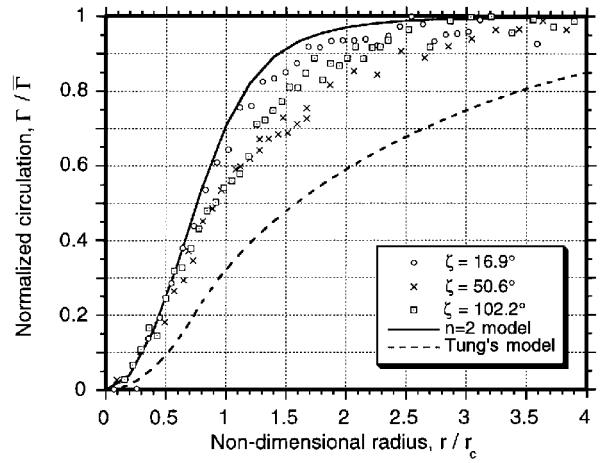

a) Linear scale

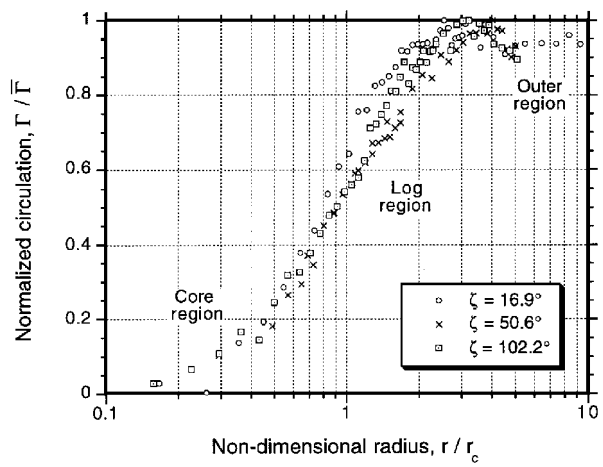

b) Log scale

Fig. 7 Circulation profiles at different wake ages.

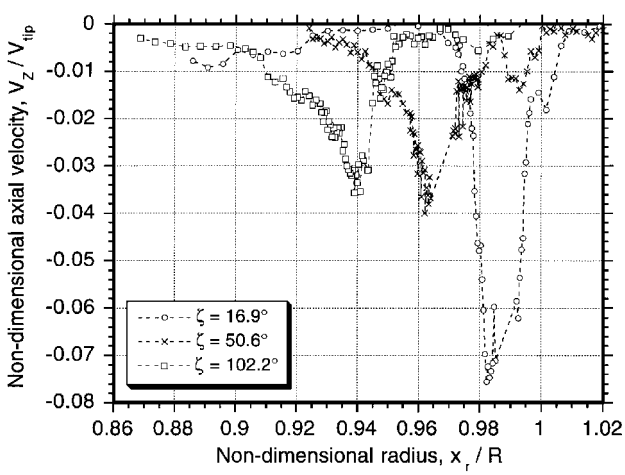

Fig. 8 Axial velocity profiles at different wake ages, plotted in the rotor coordinate system.

embedded inside the primary vortex. Evidence of such secondary vortex structures have been reported by Corsiglia et al.[14] Secondary vortices generated on rectangular rotor blade tips have also been documented by means of flow visualization.[47]

Turbulence Structure

The tip vortex, which is generated and left in the flow immediately after the passage of the blade tip, initially exhibits a laminar behavior. This is accompanied by a maximum in kinetic energy, and shortly thereafter the vortex becomes turbulent. The time scales over which this occurs are related in part to the vortex Reynolds number $\bar{\Gamma}/\nu$. The vortex is enveloped by a mixing layer, which transfers

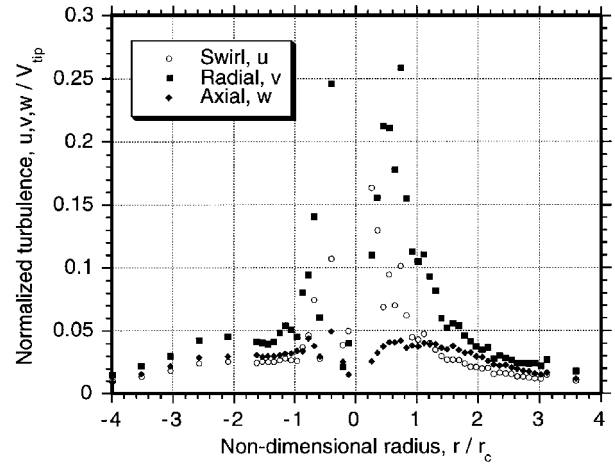

Fig. 9 Swirl, radial, and axial components of turbulence in the tip vortex at $\zeta = 16.9$ deg.

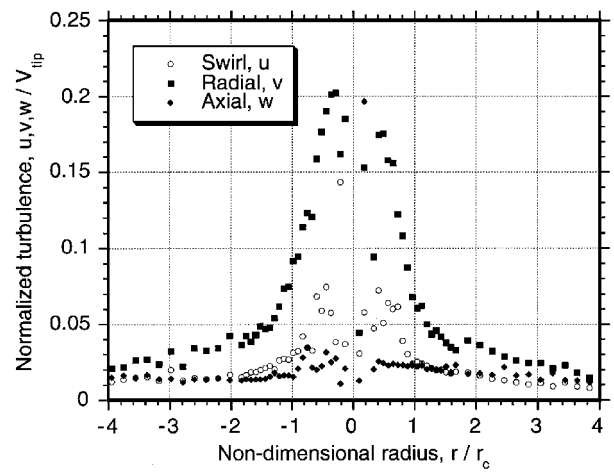

Fig. 10 Swirl, radial, and axial components of turbulence in the tip vortex at $\zeta = 50.6$ deg.

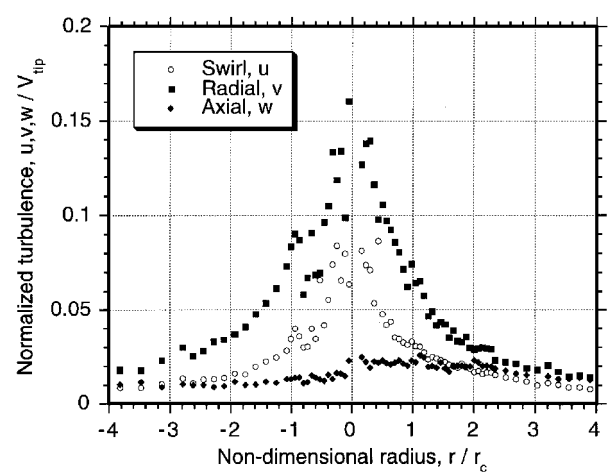

Fig. 11 Swirl, radial, and axial components of turbulence in the tip vortex at $\zeta = 102.2$ deg.

the turbulent kinetic energy contained in the vortex core into smaller eddies downstream. In these smaller eddies, the turbulent kinetic energy is ultimately dissipated by viscosity. This so-called cascading mechanism is described in detail in Ref. 48.

Turbulence Intensities

The tangential, radial, and axial turbulence components were measured at the three earliest wake ages (the results shown in Figs. 9–11). Recall that these measurements were taken in coincidence mode, that is, an equal number of statistically valid samples

were recorded for all three velocity components. Needless to say, it is very difficult to obtain true turbulence data with LDV unless special precautions are taken to use small seed particles and also to minimize the possibilities of vortex wandering. Wandering is a problem that results a random motion of the vortex trail.[11,12,30] With rotors, the problem is a little different in that an aperiodic motion of the vortex occurs with respect to some fixed blade position. Compared to a vortex generated by a fixed wing, however, this wandering issue is less of an issue for rotor measurements because both the tangential motion of the tip vortex and its helical shape have higher angular momentum and, therefore, the tip vortex maintains a more stable path. This has been verified by flow visualization,[49] although generally this can only be ensured up to the first blade passage (in this case at 360 deg of wake age). At the first blade passage, it is known that some additional aperiodicity is produced, after which spatial periodicity cannot be guaranteed with the same confidence. Fortunately, based on flow visualization it has been possible to conclude that none of the present measurements are biased by aperiodicity to any significant degree.

Certain trends in the turbulence can be expected. For example, the vortex core must be a stagnation point on a plane perpendicular to the tip vortex axis. Therefore, both the turbulence and higher moments must have peaks in both the outer (outside rotor slipstream) and inner (inside rotor slipstream) regions adjacent to the vortex core. Indeed, at wake ages of 17 and 51 deg distinct double peaks were observed in all of the axial, tangential, and radial turbulence components. If wandering was to prevail, it might be expected that a broad turbulence profile with only one distinct turbulence peak would be observed in all three components, as has been obtained in most previous measurements with fixed wings.[9,29,30] For the data obtained at 102 deg, it was difficult to identify separate turbulence peaks in both inboard and outboard regions of the vortex. However, this behavior was only observed at the oldest wake age, and even then, a single peak is not necessarily symptomatic of wandering.

The turbulence measurements made at 17 deg of wake age showed some scatter in the u (swirl) and v (radial) components near the vortex core, whereas the w (axial) component had a very smooth distribution throughout. As the tip vortex aged, all three profiles became somewhat smoother and widened radially in extent while their peaks simultaneously diminished in magnitude. In particular, note that the axial turbulence component became biased toward the inner side of the vortex, probably as a result of the energetic turbulent motion produced in the wake behind the inner part of the blade.

Using these measured turbulence data, the turbulent kinetic energy (TKE) q^2 can be derived for the three wake ages (shown in Fig. 12). The transport of TKE downstream is achieved by a balance of production, diffusion, and dissipation mechanisms, which can be seen in the TKE transport equation.[50] As expected, this composite profile looks similar to those of the individual turbulence intensities. Note, however, that the profile at 102 deg becomes somewhat more Gaussian, with the minimum found at the center of the vortex at the earlier ages now disappearing. It was also found that in all cases

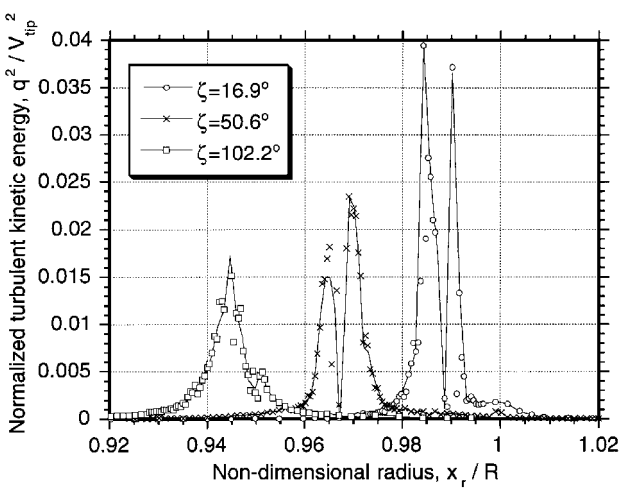

Fig. 12 Evolutionary behavior of turbulent kinetic energy in the tip vortex.

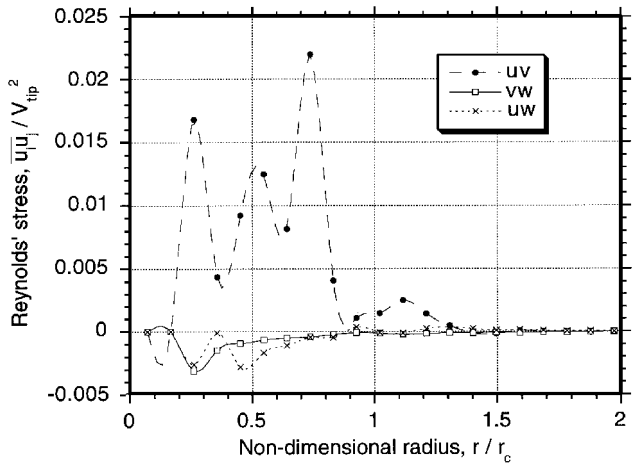

Fig. 13 Reynolds' shear stresses and spline curve fits at ζ = 16.9 deg.

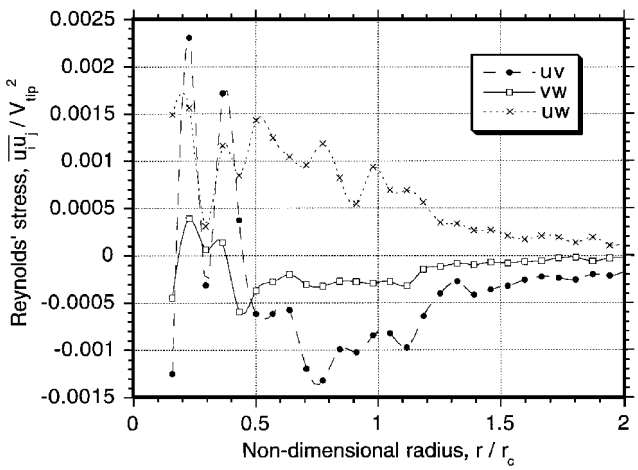

Fig. 14 Reynolds' shear stresses and spline curve fits at ζ = 102.2 deg.

most of the TKE stayed confined to within two vortex core radii and had little or no activity over $3\bar{r}$.

Several noteworthy features can be observed from these turbulence results. First, the peaks in the turbulence quantities were observed to exist significantly inside the vortex core radius, that is, inside the peaks in the tangential velocities. This confirms that turbulence is generated mostly by shear just inside the core, which is then diffused radially outward. The present results are different to those found by Tung et al.,[5] where it was reported that the results were dominated mainly by the tangential component of turbulence. In the present work, the radial component of turbulence was found to be the most dominant term.

Reynolds' Stresses

The Reynolds' shear stresses are plotted in Figs. 13 and 14, which show data for the inner (rotor slipstream) regions of the vortex flow at the earliest and latest measured wake age. Turbulent stresses were active only inside the core radius for the first two wake ages and then mostly for the youngest age. There was little or no activity beyond three-core radii for all three wake ages. The $\overline{uv}$ component was the most active, which means that both the tangential fluctuations and the radial fluctuations have dominant contributions to the generation of turbulent stresses inside the core boundaries of the vortex.

In general, there are a dearth of experimental data documenting Reynolds' shear stresses in tip vortex flows. Therefore, it is very difficult to compare the present measurements to any other data. The most extensive experimental work on Reynolds' stresses has been carried out by Phillips and Graham.[13] In their work, the Reynolds' stresses generated by imbedding a weak axial jet in a vortex resulted in wake age dependent trends. The most dominant $\overline{uv}$ component showed one peak over the positive distribution at earlier wake ages, but had both positive and negative peaks farther downstream. This trend is exactly the same as was observed in the present work, even

though the radial scales cannot be directly compared. As the vortex ages, however, the magnitudes of all the components decay in both sets of results, so that the $\overline{uw}$ and $\overline{vw}$ components become comparable to the $\overline{uv}$ components downstream. In most jet flows without swirl, the $\overline{vw}$ terms have dominant roles. Therefore, as the $\overline{vw}$ component becomes dominant or comparable in magnitude to the other terms, the tip vortex flow tends to become a simple wakelike flow and thereafter diffuses quickly.

Turbulence Production

Based on the measured Reynolds' shear stresses, it is significant to examine how turbulence is produced as the tip vortex ages. The following equation can be introduced for the turbulence production P from the turbulent kinetic energy transport equation[50]:

$$P = -\overline{u_i u_j}\frac{\partial U_i}{\partial x_j} \tag{6}$$

As can be seen in this equation, the mean strain rate, as well as the Reynolds' shear stress, contributes to turbulence. That is, the production is related to how the mean flow operates on the turbulence besides the Reynolds' stress itself. Within the assumptions of incompressible quasisteady flow, and by comparisons of orders of magnitude (see Appendix for further details), the equation for turbulence production can be approximated as

$$P = -\left[\overline{uv}\frac{\partial V_\theta}{\partial r} + \overline{uv}\frac{V_\theta}{r} - 2\overline{v^2}\frac{V_\theta}{r} + \overline{uw}\frac{\partial V_z}{\partial r}\right] \tag{7}$$

In this equation, the first three terms have a more dominant role at the creation of the vortex, and the last term increases as the vortex ages.

In the TKE transport equation it can be seen that turbulence production has different roles depending on sign changes. The resultant sign changes in Eq. (7) can be deduced from the signs of both Reynolds' shear stress and the gradient of mean velocity inside the tip vortex. Figures 13 and 14 show approximate curve fits to the Reynolds' shear stress data, where sign changes can be observed in each of the components. On one hand, the $\overline{uv}$ component had positive signs at the earliest two wake ages, and became mostly negative at $\zeta = 102$ deg. On the other hand, the $\overline{vw}$ component remained mostly negative, and the $\overline{uw}$ component became positive. The tip vortex has a severe gradient in the tangential component of velocity at the core boundary and, therefore, must produce most of the turbulence inside the vortex as a result of the product of this gradient term and the energetic $\overline{uv}$ component.

It will also be clear that substantial amounts of TKE are produced near the edge of the viscous region just outside the core region because the mean velocity gradient is still high even though Reynolds' shear stresses here are small. Furthermore, turbulence production has different mechanisms inside and outside of the core because the mean velocity gradient has different signs in each region. Therefore, for both positive signs of Reynolds' shear stress and the mean gradient, e.g., inside the core radius at the earlier wake age for the $\overline{uv}$ component in these cases, turbulence production will be generated from the mean velocity gradient, whereas outside the core the production transfers kinetic energy to the mean flow to contribute to diffusion.[48]

Calculations of TKE production using Eq. (7) have been made using the measured velocity profiles, their gradients, and the Reynolds' stresses. The resulting estimated production profiles for wake ages of 16.9, 50.6, and 102.2 deg are plotted in Fig. 15. Although the statistics are hard to acquire inside the vortex core, the TKE production quickly decreases with increasing wake age. This confirms that the mean velocity field creates significant turbulence at the earliest wake age, and diffusive action follows rather quickly within half a rotor revolution.

Clearly the diffusive characteristics of the vortex will aid in its decay downstream, thereby attenuating the induced effects on following blades. The mean kinetic energy imbedded at vortex origination enlarges the vortex core and brings it into the fast transfer to dissipation stage, mostly by pressure action. Unfortunately, because turbulent quantities related to pressure fluctuations cannot be quantified easily, an understanding of the diffusion mechanism will be provided only by the triple moments, which are challenging to obtain.

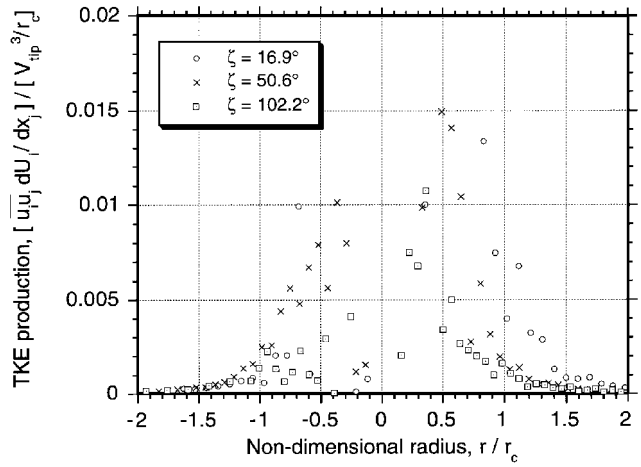

Fig. 15 TKE production at wake ages of 16.9, 50.6, and 102.2 deg.

Summary and Conclusions

The tip vortex structure generated by a rotor and its evolving behavior with respect to wake age was examined using three-component LDV. The following conclusions have been drawn from this work.

1) A strong self-similarity based on the $n = 2$ profile exists for the tangential (swirl) component of the tip vortex. This has important consequences for rotor wake models, where a single vortex model must usually be assumed.

2) The viscous core of the tip vortex was found to diffuse logarithmically with wake age, being approximately 3% of blade chord just after formation and reaching a size of approximately 13% chord at $\zeta = 311$ deg, prior to the first blade passage. During this process net vorticity contained inside the vortex core was found to remain nominally constant, confirming that dissipation was mild.

3) An average turbulent kinematic viscosity coefficient that was approximately 10 times the laminar value was found to describe the growth in the viscous core and to decrease in peak swirl velocity, at least up to the first blade passage. This result, however, will be a function of vortex Reynolds number.

4) Peaks in all three of the turbulence quantities were observed to exist significantly inside the vortex core radius, that is, inside the peaks in the tangential velocities. This confirms that turbulence is generated mostly by shear inside the viscous core of the vortex, which is then diffused radially outward.

5) The radial component of the turbulence was found to dominate inside the tip vortex. This also produces a strong contribution to the generation of Reynolds' shear stresses inside the vortex.

6) The turbulent kinetic energy production was found to exhibit a significant change within half a rotor revolution. The behavior of the vortex in these early stages will play an important role in defining the conditions of the vortex at later wake ages, perhaps where blade vortex interactions may occur.

Appendix: Approximate Turbulence Production

To investigate the TKE transport near the vortex core, the following TKE transport equation can be used:

$$U_j\frac{\partial}{\partial x_j}\left(\frac{1}{2}\overline{u_i u_j}\right) = -\frac{\partial}{\partial x_j}\left(\frac{\overline{u_j p}}{\rho} + \frac{1}{2}\overline{u_i u_i u_j} - 2\nu\overline{u_i s_{ij}}\right) - \overline{u_i u_j}S_{ij} - 2\nu\overline{s_{ij}s_{ij}} - \epsilon \tag{A1}$$

where

$$S_{ij} = \frac{1}{2}\left(\frac{\partial U_i}{\partial x_j} + \frac{\partial U_j}{\partial x_i}\right) \tag{A2}$$

where s_{ij} is the fluctuating quantity of S_{ij}, which is the strain rate of the instantaneous velocities, and

$$\epsilon = \nu\overline{\left(\frac{\partial u_i}{\partial x_j} + \frac{\partial u_j}{\partial x_i}\right)\frac{\partial u_j}{\partial x_i}} \tag{A3}$$

is the dissipation of the TKE.

In the vortex coordinate system, Eq. (A1) can be simplified with assumptions of quasisteady incompressible flow and rotational symmetry and without pressure correlation and viscous work terms to give

$$\frac{1}{2}\left(V_r \frac{\partial}{\partial r}\overline{q^2} + V_z \frac{\partial}{\partial z}\overline{q^2} \right) = -\frac{1}{2}\left(\frac{\partial}{\partial r}\overline{uq^2} + \frac{\partial}{\partial z}\overline{wq^2} + \frac{\overline{uq^2}}{r} \right) - \left(\overline{u^2}\frac{\partial V_r}{\partial r} + \overline{uw}\frac{\partial V_r}{\partial z} + \overline{v^2}\frac{V_r}{r} \overline{w^2}\frac{\partial V_z}{\partial z} + \overline{uw}\frac{\partial V_z}{\partial r} + \overline{uv}\frac{\partial V_\theta}{\partial r} + \overline{vw}\frac{\partial V_\theta}{\partial z} + \overline{uv}\frac{V_\theta}{r} - 2\overline{v^2}\frac{V_\theta}{r} \right) - \epsilon \tag{A4}$$

where

$$\overline{q^2} = \tfrac{1}{2}(\overline{u^2} + \overline{v^2} + \overline{w^2}) \tag{A5}$$

is the TKE.

Equation (A5) can be simplified further by comparing orders of magnitudes of each of the terms. In this fast rotating flow structure we can consider the flowfield to be confined by a long helical tip vortex trail and a small vortex tube whose boundary expands in the vertical direction to the trail or in the radial direction of the vortex coordinate. Therefore, the length scales Δz and Δr can be selected in the ratio $\Delta z{:}\Delta r \approx R{:}r_c$, where R is the rotor radius and r_c is the vortex core radius. In a practical sense, the relation $r_c/R \ll 1$ is valid, including this case. For velocity scales along the vortex trails the radial component V_r is much smaller than V_θ and V_z. Therefore, the following relation can be established:

$$V_\theta, V_z{:}V_r \approx \Delta z{:}\Delta r \approx R{:}r_c \tag{A6}$$

By introducing a nondimensional symbol $\delta(\ll 1)$ this equation will be

$$V_\theta, V_z{:}V_r \approx \Delta z{:}\Delta r \approx 1{:}\delta \tag{A7}$$

Equation (A4) can now be simplified by using these order of magnitude approximations, giving

$$\frac{1}{2}\left(\delta\frac{1}{\delta}\overline{q^2} + 1\frac{1}{1}\overline{q^2} \right) = -\frac{1}{2}\left(\frac{1}{\delta}\overline{uq^2} + \frac{1}{1}\overline{wq^2} + \frac{\overline{uq^2}}{\delta} \right) - \left(\overline{u^2}\frac{\delta}{\delta} + \overline{uw}\frac{\delta}{1} + \overline{v^2}\frac{\delta}{\delta} + \overline{w^2}\frac{1}{1} + \overline{uw}\frac{1}{\delta} + \overline{uv}\frac{1}{\delta} + \overline{vw}\frac{1}{1} + \overline{uv}\frac{1}{\delta} - 2\overline{v^2}\frac{1}{\delta} \right) - \epsilon \tag{A8}$$

Rearranging terms that have orders of magnitude of $1/\delta$, the following terms remain:

$$0 = -\frac{1}{2}\left(\frac{\partial}{\partial r}\overline{uq^2} + \frac{\overline{uq^2}}{r} \right) - \left(\overline{uw}\frac{\partial V_z}{\partial r} + \overline{uv}\frac{\partial V_\theta}{\partial r} + \overline{uv}\frac{V_\theta}{r} - 2\overline{v^2}\frac{V_\theta}{r} \right) - \epsilon \tag{A9}$$

This equation will be valid for fully developed vortices because the inertia terms have been ignored. The right-hand side of this equation has transport, production, and dissipation terms. The transport has triple terms, which are order of $\mathcal{O}(u^3)$, and production terms that are of $\mathcal{O}(u^2 V)$. Therefore, production will be of first order and balanced with dissipation.

Acknowledgments

Support for the first author was provided by a Yeungnam University Research Grant and by the Center for Rotorcraft Education and Research. The first author also acknowledges the support of Daewoo Heavy Industry and Advanced Fluid Engineering Research Center. The second and third authors were supported, in part, by the U.S. Army Research Office under the Rotorcraft Centers of Excellence Program, Contracts DAAH-04-93-G-001 and DAAH-04-93-G-0223. Some of this work was first presented at Forum 52 of the American Helicopter Society, Washington, DC, June 4–6, 1996.

References

[1]Schmitz, F. H., "Rotor Noise," *Aeroacoustics of Flight Vehicles: Theory and Practice*, Vol. 1, NASA Reference Publication 1258, Aug. 1991, Chap. 2.

[2]Dawson, S., Hassan, A., Straub, F., and Tadghighi, H., "Blade-Mounted Flap Control of BVI Noise Reduction Proof-of-Concept Test," NASA Rept. 195078, July 1995.

[3]Crouse, G. L., Leishman, J. G., and Bi, N., "Theoretical and Experimental Study of Unsteady Rotor/Body Aerodynamic Interactions," *Journal of the American Helicopter Society*, Vol. 37, No. 1, 1992, pp. 55–64.

[4]Torok, M. S., and Ream, D. T., "Investigation of Empennage Airloads Induced by a Helicopter Main Rotor Wake," American Helicopter Society 49th Annual Forum, St. Louis, MO, May 1993.

[5]Tung, C., Pucci, S. L., Caradonna, F. X., and Morse, H. A., "The Structure of Trailing Vortices Generated by Model Rotor Blades," *Vertica*, Vol. 7, No. 1, 1983, pp. 33–43.

[6]Singh, P. I., and Uberoi, M. S., "Experiments on Vortex Stability," *Physics of Fluids*, Vol. 19, No. 12, 1976, pp. 1858–1863.

[7]Bandyopadhyay, P. R., Stead, D. J., and Ash, R. L., "Organized Nature of a Turbulent Trailing Vortex," *AIAA Journal*, Vol. 29, No. 10, 1991, pp. 1627–1633.

[8]Leuchter, O., and Solignac, J. L., "Experimental Investigation of the Turbulent Structure of Vortex Wakes," *Proceedings of Turbulent Shear Flows 4*, Springer–Verlag, Berlin, 1983, p. 531.

[9]Sarpkaya, T., and Neubert, D. E., "Interaction of a Streamwise Vortex with a Free Surface," *AIAA Journal*, Vol. 32, No. 3, 1994, pp. 594–600.

[10]Cutler, A. D., and Bradshaw, P., "A Crossed Hot-Wire Technique for Complex Turbulent Flows," *Experiments in Fluids*, Vol. 12, 1991, pp. 17–22.

[11]Devenport, W. J., Rife, M. C., Liapis, S. I., and Follin, G. J., "Turbulence Structure and Scaling in Trailing Vortices," AIAA Paper 95-0588, Jan. 1995.

[12]Devenport, W. J., Rife, M. C., Liapis, S. I., and Follin, G. J., "The Structure and Development of a Wing-Tip Vortex," *Journal of Fluid Mechanics*, Vol. 312, 1996, pp. 67–106.

[13]Phillips, W. R. C., and Graham, A. H., "Reynolds' Stress Measurements in a Turbulent Trailing Vortex," *Journal of Fluid Mechanics*, Vol. 147, 1984, pp. 353–371.

[14]Corsiglia, V. R., Schwind, R. G., and Chiglier, N. A., "Rapid Scanning, Three-Dimensional Hot Wire Anemometer Surveys of Wing-Tip Vortices," *Journal of Aircraft*, Vol. 22, No. 2, 1985, pp. 158–160.

[15]Cook, C. V., "The Structure of the Rotor Blade Tip Vortex," *Aerodynamics of Rotary Wings*, AGARD CP-111, Sept. 1972 (Paper 3).

[16]Landgrebe, A. J., and Bellinger, E. D., "An Investigation of the Quantitative Applicability of Model Helicopter Rotor Wake Patterns Obtained from a Water Tunnel," United Aircraft Research Lab., UARL K910917-23, Dec. 1971.

[17]Landgrebe, A. J., "The Wake Geometry of a Hovering Rotor and Its Influence on Rotor Performance," *Journal of the American Helicopter Society*, Vol. 17, No. 4, 1972, pp. 2–15.

[18]Sullivan, J. P., "An Experimental Investigation of Vortex Rings and Helicopter Rotor Wakes Using a Laser Doppler Velocimeter," Aerophysics Lab., Massachusetts Inst. of Technology, TR 183, MIT DSR 80038, Cambridge, MA, June 1973.

[19]Bagai, A., and Leishman, J. G., "Flow Visualization of Compressible Vortex Structures Using Density Gradient Techniques," *Experiments in Fluids*, Vol. 15, 1993, pp. 431–442.

[20]Leishman, J. G., Baker, A., and Coyne, A., "Measurements of Rotor Tip Vortices Using Three-Component Laser Doppler Velocimetry," *Journal of the American Helicopter Society*, Vol. 41, No. 4, 1996, pp. 342–353.

[21]McAlister, K. W., Schuler, C. A., Branum, L., and Wu, J. C., "3-D Wake Measurements near a Hovering Rotor for Determining Profile and Induced Drag," NASA TP 3577, Aug. 1995.

[22]Seelhorst, U., Beesten, B. M. J., and Bütefisch, K. A., "Flowfield Investigation of a Rotating Helicopter Rotor Blade by Three-Component Laser Doppler Velocimetry," 75th AGARD Fluid Dynamics Panel Symposium, Berlin, Oct. 1994.

[23]Biggers, J. C., and Orloff, K. L., "Laser Velocimeter Measurements of the Helicopter Rotor-Induced Flow Field," American Helicopter Society 30th Annual Forum, Washington, DC, May 1974.

[24]Biggers, J. C., Chu, S., and Orloff, K. L., "Laser Velocimeter Measurements of Rotor Blade Loads and Tip Vortex Rollup," American Helicopter Society 31st Annual Forum, Washington, DC, May 1975.

[25]Owen, K. F., and Tauber, M. E., "Measurement and Prediction of Model Rotor Flowfields," *Journal of Aircraft*, Vol. 23, No. 11, 1986, pp. 843–851.

[26]Buchhave, P., George, W. K., and Lumley, J. L., "The Measurement of Turbulence with the Laser Doppler Anemometer," *Annual Review of Fluid Mechanics*, Vol. 11, 1979, pp. 443–503.

[27]Adrian, R. J., *Laser Velocimetry Fluid Mechanics Measurements*, Hemisphere, New York, 1983, pp. 155–244.

[28]Orloff, K. L., "Trailing Vortex Wind Tunnel Diagnostics with a Laser Velocimeter," *Journal of Aircraft*, Vol. 11, No. 8, 1974, pp. 477–482.
[29]Takahashi, R. K., and McAlister, K. W., "Preliminary Study of a Wing-Tip Vortex Using Laser Velocimetry," NASA TM 88343, Jan. 1987.
[30]McAlister, K. W., and Takahashi, R. K., "NACA 0012 Wing Pressure and Trailing Vortex Measurements," NASA TP 3151, Nov. 1991.
[31]Thompson, H. D., and Stevenson, W. H. (Eds.), *Laser Velocimetry and Particle Sizing*, Hemisphere, New York, 1978, pp. 7, 50–63, 171–175.
[32]Leishman, J. G., "On Seed Particle Dynamics in Tip Vortex Flows," *Journal of Aircraft*, Vol. 33, No. 4, 1996, pp. 823, 824.
[33]Thomson, T. L., Komerath, N. M., and Gray, R. B., "Visualization and Measurement of the Tip Vortex Core of a Rotor Blade in Hover," *Journal of Aircraft*, Vol. 25, No. 2, 1988, pp. 1113–1121.
[34]Chigier, N. A., and Corsiglia, V. R., "Tip Vortices—Velocity Distributions," American Helicopter Society 27th Annual Forum, Washington, DC, May 1971.
[35]Payne, P. R., *Helicopter Dynamics and Aerodynamics*, Macmillan, New York, 1959, p. 87.
[36]Bliss, D. B., Quackenbush, T. R., and Bilanin, A. J., "A New Methodology for Helicopter Free-Wake Analyses," *Proceedings of the 39th Annual Forum of the American Helicopter Society*, American Helicopter Society, Washington, DC, 1983.
[37]Vatistas, G. H., Kozel, V., and Mih, W. C., "A Simpler Model for Concentrated Vortices," *Experiments in Fluids*, Vol. 11, No. 1, 1991, pp. 73–76.
[38]Lamb, H., *Hydrodynamics*, 6th ed., Cambridge Univ. Press, New York, 1932, pp. 592, 593, 668, 669.
[39]Bagai, A., and Leishman, J. G., "Rotor Free-Wake Modeling Using a Relaxation Technique—Including Comparisons with Experimental Data," *Journal of the American Helicopter Society*, Vol. 40, No. 3, 1995, pp. 29–41.
[40]Bagai, A., and Leishman, J. G., "Rotor Free-Wake Modeling Using a Pseudo-Implicit Relaxation Algorithm," *Journal of Aircraft*, Vol. 32, No. 6, 1995, pp. 1276–1285.
[41]Leonard, A., "Vortex Methods for Flow Simulation," *Journal of Computational Physics*, Vol. 37, No. 3, 1980, pp. 289–335.
[42]Johnson, G. M., "Research on the Propagation and Decay of Vortex Rings," Aeronautical Research Lab., ARL 70-0093, June 1970.
[43]Ogawa, A.,*Vortex Flow*, Series on Fine Particle Science and Technology, CRC Press, Boca Raton, FL, 1993, pp. 193–196.
[44]Dosanjh, D. S., Gasparek, E. P., and Eskinazi, S., "Decay of Viscous Trailing Vortex," *Aeronautical Quarterly*, Vol. 13, May 1962, pp. 167–188.
[45]Squire, H. B., "The Growth of a Vortex in Turbulent Flow," *Aeronautical Quarterly*, Vol. 16., Aug. 1965, pp. 302–306.
[46]Schlichting, H., *Boundary Layer Theory*, 7th ed., McGraw–Hill, New York, 1979, pp. 747–750.
[47]Bagai, A., and Leishman, J. G., "A Study of Rotor Wake Development and Wake/Body Interactions in Hover," *Journal of the American Helicopter Society*, Vol. 37, No. 4, 1992, pp. 48–57.
[48]Tennekes, H., and Lumley, J. L., *A First Course in Turbulence*, MIT Press, Cambridge, MA, 1972, pp. 256–275.
[49]Moedersheim, E., Daghir, M., and Leishman, J. G., "Flow Visualization of Rotor Wakes Using Shadowgraph and Schlieren Techniques," 20th European Rotorcraft Forum, Paper 31, Amsterdam, The Netherlands, Oct. 1994.
[50]Hinze, O. J., *Turbulence*, McGraw–Hill, New York, 1959.

S. Glegg
Associate Editor